



Contents lists available at ScienceDirect

## Journal of Magnetism and Magnetic Materials

journal homepage: [www.elsevier.com/locate/jmmm](http://www.elsevier.com/locate/jmmm)

## Research article

Pulsating magnetohydrodynamic flow of  $\text{Fe}_3\text{O}_4$ -blood based micropolar nanofluid between two vertical porous walls with Cattaneo–Christov heat flux and entropy generationD. Rajkumar <sup>a,b</sup>, A. Subramanyam Reddy <sup>a,\*</sup>, P.V. Satya Narayana <sup>a</sup>, K. Jagadeshkumar <sup>a</sup>, Ali J. Chamkha <sup>c</sup><sup>a</sup> Department of Mathematics, School of Advanced Sciences, Vellore Institute of Technology, Vellore 632014, Tamil Nadu, India<sup>b</sup> Department of Mathematics, Sathyabama Institute of Science and Technology, Chennai 600119, India<sup>c</sup> Faculty of Engineering, Kuwait College of Science and Technology, Doha District 35004, Kuwait

## ARTICLE INFO

## Keywords:

Pulsatile flow  
Micropolar nanofluid  
Entropy generation  
Thermal radiation  
Joule heating  
MHD

## ABSTRACT

The present article is aimed to investigate the impact of entropy generation on pulsating hydromagnetic flow of a micropolar nanofluid between two vertical porous walls using the Cattaneo–Christov heat flux model. Here  $\text{Fe}_3\text{O}_4$  (magnetite) is taken as a nanoparticle and blood as micropolar fluid (base fluid). The significance of viscous dissipation, Ohmic heating, and thermal radiation are considered. This model is noteworthy in the field of magnetic bioseparation, pressure surges, magnetofection agent, biomedical engineering, cancer therapeutic, artificial kidney, brain tumors, and nano-drug delivery in the arteries. The governing partial differential equations are transformed into the system of ordinary differential equations by deploying the perturbation process and then solved numerically by employing the fourth-order Runge–Kutta scheme with the support of the shooting technique. The flow variables like velocity, microrotation, temperature, entropy generation, and Bejan number are depicted graphically and discussed in detail. The heat transfer rate is displayed through a table. The results depict that the velocity is diminishing with the enhancement of coupling parameter, Hartmann number, and nanoparticle volume fraction. The temperature of micropolar nanofluid is increasing with an increment of viscous dissipation, thermal radiation, and heat source while it is reducing with the enhancement of magnetic field, thermal relaxation time, and heat sink parameter. The entropy generation is diminished by increasing the values of Hartmann number, thermal relaxation, and coupling parameter. Further, the Bejan number is enhanced by varying thermal radiation and nanoparticle volume fraction.

## 1. Introduction

Nowadays, the micropolar nanofluid model is widely used in research aspect. Such non-Newtonian fluids exhibit specific nano effects and microstructures. The theory of micropolar fluid was initialized by Eringen [1,2] later he extended that into thermo-micro stretch fluid and bubbly liquids [3]. The particles in the micropolar fluid are rigid and randomly oriented. For such a fluid, the spin vector and microinertia tensor are also required so that stress moments can be supported by body couplings. Micropolar fluids have the potential to have many physical manifestations, including liquid crystals, bubbly liquids, polar fluids, colloidal solutions, animal blood, polymeric fluids, and dumbbell molecules. Shah et al. [4] examined the Darcy–Forchheimer flow of micropolar ferrofluid through Cattaneo–Christov heat flux model with effects of thermal radiation, external electric field exposed to both suction and injection walls. Nadeem et al. [5] analyzed an incompressible

micropolar nanofluid with microorganisms over a stretching sheet on a three-dimensional unsteady forced bioconvective flow. Ellahi. [6] discussed the magnetohydrodynamic flow of non-Newtonian nanofluid in a pipe with temperature dependent viscosity using homotopy analysis method. Si et al. [7] studied the micropolar nanofluid flow and heat transfer via channel with the effects of viscous dissipation in a channel by using the Homotopy analysis method. Pal et al. [8] obtained the influences of thermal radiation and heat source/sink on hydromagnetic electrically leading on micropolar nanofluid flow through stretching sheet by utilizing the Runge–Kutta Fehlberg approach along with shooting technique. Vasu et al. [9] deliberated the unsteady two-dimensional pulsating micropolar blood flow in a tapered artery by employing the finite element method. Also, this analysis is motivated by using nano-drug delivery applications. Jaiswal and Yadav [10] investigated the

\* Corresponding author.

E-mail address: [anala.subramanyamreddy@gmail.com](mailto:anala.subramanyamreddy@gmail.com) (A. Subramanyam Reddy).<https://doi.org/10.1016/j.jmmm.2023.170564>

Received 15 June 2022; Received in revised form 19 January 2023; Accepted 20 February 2023

Available online 1 March 2023

0304-8853/© 2023 Elsevier B.V. All rights reserved.

two-phase model on a micropolar Newtonian in a blood flow artery over a circular cylindrical tube including uniform magnetic field and coupling parameter. This work is maybe suitable for various medical reasons. Zeeshan et al. [11] dealt with the electromagnetic flow of *SWCNT/MWCNT* of engine oil based carbon nanotubes over porous media. Aslani et al. [12] explored the influence of micromagnetorotation on hydromagnetic micropolar Poiseuille flow between two infinite plates and this may be useful for various enormous applications like bioengineering which contains micropolar fluids and industrials.

In the last two decades, researchers have endeavored the nanofluid which plays a vital role in science, engineering, and technology for impressive applications like cooling processes, mechanical systems, biomedical, drug delivery, nanofabrication, oil recovery, and so on. The term nanofluid was first proposed by Choi [13] and he established the results of heat transfer fluids which can be engineered by suspending metallic nanoparticles in conservative heat transfer fluids and gives better heat transfer. Wahed et al. [14] studied the Ohmic heating effect on Ferro-nanofluid fluid flow in a curved tube with the impacts of hall current by employing Differential transformation method (DTM) with associated of Pade approximation technique. Ghadikolaei et al. [15] studied an incompressible micropolar nanofluid through the iron oxide, ferro-ethylene glycol nanoparticles on hydro-magnetic boundary layer flow in a porous medium in a stretching sheet with the presence of Ohmic heating and thermal effects. Sheikholeslami et al. [16] examined the influence of radiation effect on MHD nanofluid flow and energy transfer with effects of Brownian motion and thermophoresis. Shehzad et al. [17] examined the influence of ferromagnetic and titanium allow nanoparticles in non-Newtonian micropolar fluid flow and also in this model, the Cattaneo Christov heat flux model have explored for the reason of heat transfer in a nanofluid. Hazarika et al. [18] examined the magnetohydrodynamic fluid movement with water-based nanoliquid of Ferrous Ferric Oxide, Copper (Cu), and Silver (Ag) nanoparticles past a stretchable porous sheet with viscous dissipation, Soret number, and heat generation by using Runge–Kutta fourth-order approach along with shooting technique. Venkatesan and Reddy [19] developed the pulsative magnetohydrodynamic fluid movement of Oldroyd-B nanofluid into the dynamic forces of blood assigning alumina nanoparticles in a horizontal channel over the impacts of thermal radiative and viscous dissipation. Such work is significant in engineering and biological aspects. Hassan et al. [20] discussed the nanoparticle shape factor effects on ferrofluids flow and energy transport over low oscillating magnetic field using HAM method. Hayat et al. [21] explored the bioconvective and Hall current investigation of peristaltic nanofluid over gyrotactic microorganisms with the impacts of chemical reactive and Brownian motion in a channel walls such as symmetric and elastic. Rajamani and Reddy [22] discussed the impacts of thermal radiation, heat source/sink, and Ohmic heating on pulsating flow of couple stress nanoliquid with blood carrying alumina nanoparticles in a channel by approaching the perturbation process. This process is maybe useful for nanodrug delivery, pharmaceutical, and various biological motives. Shehzad et al. [23] explored the MHD flow on a multilayer coatings fully developed with steady Newtonian and non-Newtonian fluids through parallel inclined plates in a inclined rotating channel. Sharma et al. [24] addressed with the heat transfer and entropy analysis of hydromagnetic slip flow over hybrid nanoparticles such as alumina and gold with the effects of viscous dissipation Ohmic heating, and thermal radiation by applying Crank–Nicolson scheme.

In the past few years, researchers have been looking into pulsatile flow due to its numerous innovative applications in engineering, biomedical, and industrial operations. The considered flow is studied because by inducing the pressure gradient in circular pipes or stenosed arteries and it causes to fluctuate sinusoidally. For example, in real situations we considering various emerging applications such as respiratory systems, circulatory systems, internal combustion engines, the discharge of any piston pump, control systems, and so [25–32].

Shit et al. [33] studied heat transfer and pulsating flow in a blood based porous constricted artery over the impacts of imposed magnetic field, viscous dissipation, and body force by taking Crank–Nicolson finite approach. Kumar et al. [34] studied the pulsative magnetohydrodynamic flow of Casson nanofluid through vertical permeable walls by utilizing Buongiorno's nanofluid approach over the influences of viscous dissipation and thermal radiative effects. This model is significant in biomedical, science, and technological aspects. Rajkumar and Reddy [35] studied the pulsating hydromagnetic of *Au/SWCNTs* with blood-based micropolar nanoliquid flow along with impacts of heat source/sink and viscous through a porous horizontal channel also such work helpful for biofluid modeling, human cancer treatment, and nano-drug transport. Kot and Elmabound [36] investigated the heat transfer of unsteady pulsating blood flow over stenosed artery through Cattaneo Christov model with the effects of body force, heat source, and thermal radiation by utilizing Laplace and finite Hankel transformations approach. Govindarajulu and Reddy [37] Recently, inspected the hydromagnetic hybrid third-grade nanofluid via a porous walls including the impacts of viscous dissipation, thermal radiative, and Joule heating effects by taking fourth-order Runge–Kutta procedure. Such investigation is substantial in cancer therapeutic, and the purpose of biomedical aspect for nano-drug delivery in arteries.

The consideration of the Cattaneo–Christov heat flux pattern is the purpose of effective heat transfer enhancement in the field of engineering and industrial processes. Cattaneo [38] established Fourier's model for the enrichment of energy transport and approaching different materials for having various thermal relaxation times. Also, Christov [39] proposed an invariant formulation of Maxwell–Cattaneo law for the relaxation rate of the heat flux. Such a model is suitable for the analysis of larger heat transfer rate. Rauf et al. [40] studied the unsteady hydromagnetic flow of a micropolar fluid through a periodic oscillation of a rotating disk with Cattaneo–Christov heat flux model by using successive over-relaxation approach along with finite difference scheme. Majeed et al. [41] examined the energy transport behavior over porous media of magnetite ( $Fe_3O_4$ ) nanoparticle suspended over conventional fluids by adopting the similarity transform procedure and then solving by an effective shooting algorithm. Yahya et al. [42] investigated the consequence of the Bio-convection and Cattaneo–Christov model on Williamson nanofluid via stretching surface with radiation heat flux, and convective boundary conditions. Thermal radiation influence is obtained in many different fields, including solar and power technologies, energy transporters, nuclear reactors, spacecraft, etc. [43–46]. The presence of heat source/sink is significant in various fields like chemical engineering, biomedical reasons like metallic sheets cooling, oil retrieval, and so on. Wahed [47] studied the impacts of ferromagnetic-nanofluid on a boundary layer fluid flow in a stretching sheet over the impacts like Ohmic dissipation, non-linear thermal radiation and hall current parameters. Khaled et al. [48] explored the applications of heat source/sink for thermal significances of the Brinkman micropolar nanofluid in the existence of micro-organisms.

Entropy generation analysis is widely used in engineering, biology, and industry. Such an assessment is useless because it only initiates the critical level of irreversibility in a thermal system, which requires a significant amount of energy to achieve. Different mechanisms, such as solar thermal energy, natural convection, electro-chemical, and air filters, all result in a decrease in entropy creation. Generally, Ohmic heating, viscous dissipation, and non-linear or linear thermal radiation can be applied for entropy generation (irreversibility) in thermal progressions [49,50]. Yusuf et al. [51] examined the irreversibility process in micropolar fluid with a semi-analytical solution in a heated inclined porous space following slip conditions. Hayat et al. [52] investigated the entropy analysis of hydromagnetic flow via rotating disk by utilizing of viscous dissipation and Joule heating effects. Chen and Jian [53] performed an analytical study for two immiscible fluids in a heat transfer scheme based on an entropy generation minimization approach.

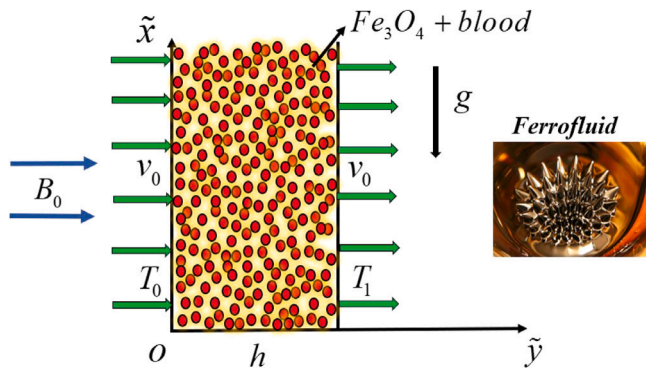


Fig. 1. Physical model of the flow problem.

Table 1

The physical and thermal features of  $Fe_3O_4$  nanoparticle and blood [45,47].

Property	$Fe_3O_4$	Blood
$C_p$ (J/(kg K))	670	3617
$k$ (W/(mK))	6	0.52
$\rho$ (kg/m <sup>3</sup> )	5200	1050
$\sigma$ ( $\Omega$ m) <sup>-1</sup>	25000	0.8
$\beta$ (1/K)	$1.3 \times 10^{-5}$	$1.8 \times 10^{-6}$

$$\frac{\partial \bar{T}}{\partial \bar{t}} + v_0 \frac{\partial \bar{T}}{\partial \bar{y}} + \lambda_2 \left( \frac{\partial^2 \bar{T}}{\partial \bar{t}^2} + v_0^2 \frac{\partial^2 \bar{T}}{\partial \bar{y}^2} + 2v_0 \frac{\partial^2 \bar{T}}{\partial \bar{y} \partial \bar{t}} \right) = \frac{k_{nf}}{(\rho C_p)_{nf}} \frac{\partial^2 \bar{T}}{\partial \bar{y}^2} + \frac{\mu_{nf} + K_1}{(\rho C_p)_{nf}} \left( \frac{\partial \bar{u}}{\partial \bar{y}} \right)^2 + \frac{\sigma_{nf} B_0^2}{(\rho C_p)_{nf}} \bar{u}^2 - \frac{1}{(\rho C_p)_{nf}} \frac{\partial q_r}{\partial \bar{y}} + \frac{Q_0}{(\rho C_p)_{nf}} (\bar{T} - T_0). \quad (3)$$

Here,  $\bar{P}$  is the fluid pressure,  $\bar{u}$  is velocity in  $\bar{x}$ -direction.  $k_{nf}$ ,  $(\rho C_p)_{nf}$ ,  $\mu_{nf}$ ,  $g(\rho\beta)_{nf}$ ,  $\rho_{nf}$ , and  $\sigma_{nf}$ , thermal conductivity, effective specific heat, dynamic viscosity, thermal expansion coefficient, density of nanofluid, and electrical conductivity of nanofluid accordingly.  $K_1$  is coupling parameter,  $j$  is microinertia parameter,  $q_r$  is the radiative heat flux,  $\bar{T}$  is the temperature of nanofluid  $\bar{N}$  is microrotation vector,  $\lambda_2$  is thermal relaxation time,  $\bar{t}$  dimensional time,  $Q_0$  is the coefficient of the heat source/sink.

The appropriate boundary conditions(B.Cs) are

$$u^*(0) = 0, \quad N^*(0) = 0, \quad T^*(0) = T_0, \quad (4)$$

$$u^*(h) = 0, \quad N^*(h) = 0, \quad T^*(h) = T_1. \quad (5)$$

The distance between the walls is denoted as  $h$  here.

The thermal properties of ferro-nanofluid are defined as follows: [18, 24],

$$\left. \begin{aligned} (\rho C_p)_{nf} &= (1 - \phi)(\rho C_p)_f + \phi(\rho C_p)_s; \\ \rho_{nf} &= (1 - \phi)\rho_f + \phi\rho_s; \\ \mu_{nf} &= \frac{\mu_f}{(1 - \phi)^{2.5}}; \\ (\rho\beta)_{nf} &= (1 - \phi)(\rho\beta)_f + \phi(\rho\beta)_s; \\ \frac{\sigma_{nf}}{\sigma_f} &= 1 + \frac{3(\frac{\sigma_s}{\sigma_f} - 1)\phi}{(\frac{\sigma_s}{\sigma_f} + 2) - (\frac{\sigma_s}{\sigma_f} - 1)\phi}; \\ \frac{k_{nf}}{k_f} &= \frac{k_s + 2k_f - 2\phi(k_f - k_s)}{k_s + 2k_f + \phi(k_f - k_s)}; \end{aligned} \right\} \quad (6)$$

here, the subscripts  $nf$ ,  $f$ , and  $s$  represent the nanofluid, base fluid, and solid nanoparticles respectively.  $\phi$  is the nanoparticle volume fraction. The thermal features of base fluid and nanoparticles are shown in Table 1. Presently, by utilizing the Rosseland approximation towards the radiative heat flux  $qr$  accordingly [24,34] and Eq. (3) becomes,

$$\frac{\partial \bar{T}}{\partial \bar{t}} + v_0 \frac{\partial \bar{T}}{\partial \bar{y}} + \lambda_2 \left( \frac{\partial^2 \bar{T}}{\partial \bar{t}^2} + v_0^2 \frac{\partial^2 \bar{T}}{\partial \bar{y}^2} + 2v_0 \frac{\partial^2 \bar{T}}{\partial \bar{y} \partial \bar{t}} \right) = \frac{k_{nf}}{(\rho C_p)_{nf}} \frac{\partial^2 \bar{T}}{\partial \bar{y}^2} + \frac{1}{(\rho C_p)_{nf}} \left[ \frac{16\bar{\sigma}}{3k} T_1^3 \frac{\partial^2 \bar{T}}{\partial \bar{y}^2} \right] + \frac{\mu_{nf} + K_1}{(\rho C_p)_{nf}} \left( \frac{\partial \bar{u}}{\partial \bar{y}} \right)^2 + \frac{\sigma_{nf} B_0^2}{(\rho C_p)_{nf}} \bar{u}^2 + \frac{Q_0}{(\rho C_p)_{nf}} (\bar{T} - T_0). \quad (7)$$

Here, Stefan–Boltzmann constant is  $\bar{\sigma}$ , and the mean absorption coefficient is  $\bar{k}$ .

Above stated studies witness that, the researchers have investigated the magnetohydrodynamic flow of various non-Newtonian nanofluid flow with some effects but the impacts of hydromagnetic pulsating micropolar nanofluid with ferromagnetic nanoparticles have not considered so far. So, the current study aims to analyze the entropy generation on pulsating magnetohydrodynamic of ferromagnetic blood-based micropolar nanofluid flow between two porous vertical walls in the presence of viscous dissipation, Joule heating, thermal radiation, and heat source/sink. Such nanoparticle magnetite ( $Fe_3O_4$ ) is an excellent candidate in the biomedical point of view like magnetic bioseparation, magnetofection agent, DNA molecule detection, hyperthermia, tissue engineering and targeted drug delivery. Here Cattaneo–Christov radiative heat flux model is utilized to examine the behavior of thermal relaxation, Bejan number and entropy generation for an irreversibility process in the energy equation. This model effectively plays a vital role in science, engineering, and medical fields like cancer treatment, nano-drug delivery in arteries, coronary artery disease, injecting medicine into the veins blood, and pharmaceuticals. Here, the perturbation process is used to turn the flow regulating partial differential equations into a system of ordinary differential equations, which is then solved using the fourth-order Runge–Kutta approach with the help of the shooting technique. The numerical outcomes were taken into account for influences of velocity, microrotation, temperature, entropy analysis and heat transfer rate. Finally, this is because of their tremendous modern applicability, this new type of research will fascinate many more scientists, encouraging us to smash down the existing conflict.

## 2. Formulation of the problem

In this work, we considered a laminar and incompressible pulsatile flow of electrically processed micropolar nanofluid between two vertical porous walls with the presence of Cattaneo–Christov heat flux model. In this segment magnetite ( $Fe_3O_4$ ) taken as nanoparticle and blood is treated as base fluid which is non-Newtonian. A coordinate system and flow model of the problem is shown in Fig. 1. The  $\bar{x}$ -axis coincides with the left wall while the  $\bar{y}$ -axis is normal to the walls. An applied magnetic field of strength  $B_0$  is imposed consistently normal to both the walls. The induced magnetic field is neglected.  $T_1$  and  $T_0$  are temperature at the right and left walls accordingly ( $T_0 < T_1$ ). Under these assumptions the governing equations are [20,26,28,31,34,37]

$$\frac{\partial \bar{u}}{\partial \bar{t}} + v_0 \frac{\partial \bar{u}}{\partial \bar{y}} = -\frac{1}{\rho_{nf}} \frac{\partial \bar{P}}{\partial \bar{x}} + \left( \frac{\mu_{nf} + K_1}{\rho_{nf}} \right) \frac{\partial^2 \bar{u}}{\partial \bar{y}^2} - \frac{\sigma_{nf} B_0^2}{\rho_{nf}} \bar{u} + \frac{g(\rho\beta)_{nf}}{\rho_{nf}} (\bar{T} - T_0) + \frac{K_1}{\rho_{nf}} \frac{\partial \bar{N}}{\partial \bar{y}}, \quad (1)$$

$$\frac{\partial \bar{N}}{\partial \bar{t}} + v_0 \frac{\partial \bar{N}}{\partial \bar{y}} = -\frac{1}{\rho_{nf} j} 2K_1 \bar{N} - \frac{K_1}{\rho_{nf} j} \frac{\partial \bar{u}}{\partial \bar{y}} + \frac{\gamma}{\rho_{nf} j} \frac{\partial^2 \bar{N}}{\partial \bar{y}^2}, \quad (2)$$

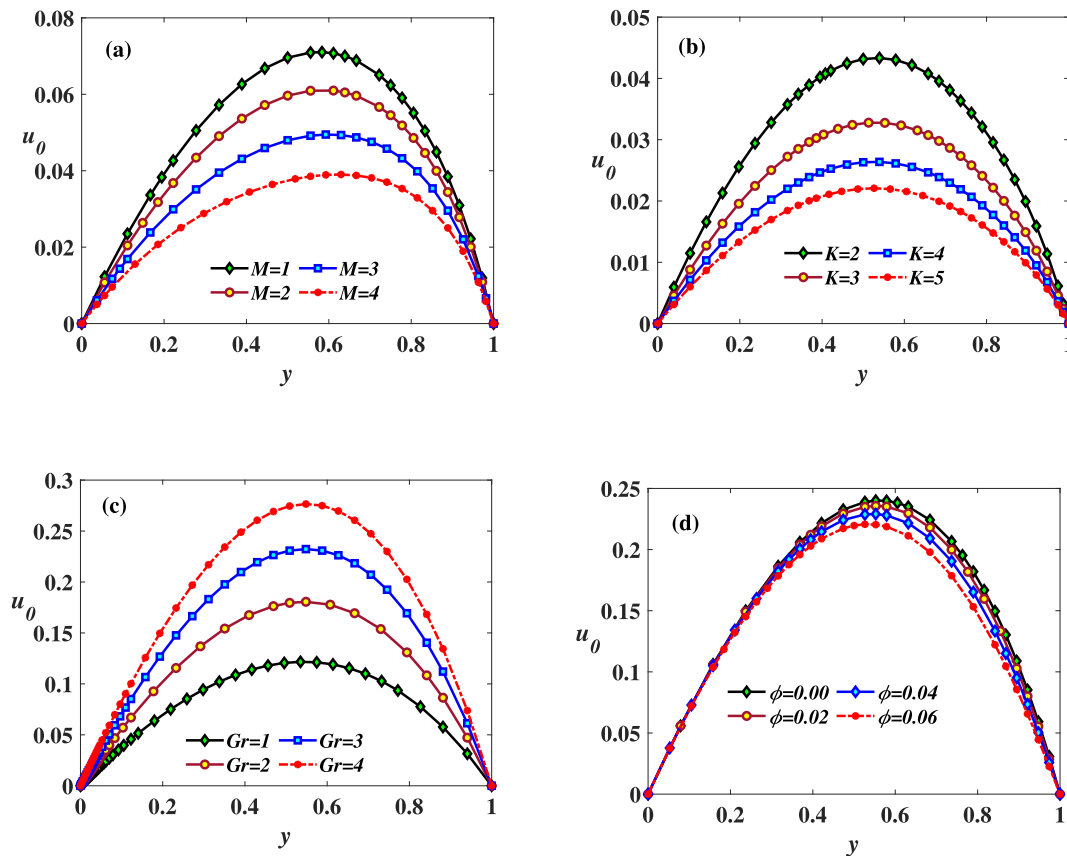


Fig. 2. (a) Impact of  $M$  on  $u_0$  (b) Impact of  $K$  on  $u_0$  (c) Impact of  $Gr$  on  $u_0$  (d) Impact of  $\phi$  on  $u_0$ .

Now, by applying the succeeding dimensionless parameters,

$$\left. \begin{aligned} u &= \frac{\tilde{u}}{v_0}, \quad x = \frac{\tilde{x}}{h}, \quad y = \frac{\tilde{y}}{h}, \quad N = \frac{\tilde{N}h}{v_0}, \quad t = \omega\tilde{t}, \quad P = \frac{h\tilde{P}}{\mu v_0} \\ Re &= \frac{v_0 h}{\nu_f}, \quad Gr = \frac{g\beta_f(T_1 - T_0)h^3}{\nu_f^2}, \quad \theta = \frac{\tilde{T} - T_0}{T_1 - T_0} \end{aligned} \right\} \quad (8)$$

Eqs. (1),(2), and (7) becomes,

$$H^2 \frac{\partial u}{\partial t} + R \frac{\partial u}{\partial y} = -\frac{1}{A_1} \frac{\partial P}{\partial x} + \left(\frac{A_2 + K}{A_1}\right) \frac{\partial^2 u}{\partial y^2} - \frac{A_5}{A_1} M^2 u + \frac{K}{A_1} \frac{\partial N}{\partial y}, \quad (9)$$

$$H^2 \frac{\partial N}{\partial t} + R \frac{\partial N}{\partial y} = -\frac{2nN}{P_j A_1} - \frac{n}{P_j A_1} \frac{\partial u}{\partial y} + \frac{1}{P_j A_1} \frac{\partial^2 N}{\partial y^2} + \frac{A_6}{A_1} \left(\frac{Gr}{Re}\right) \theta, \quad (10)$$

$$\begin{aligned} H^2 \frac{\partial \theta}{\partial t} + R \frac{\partial \theta}{\partial y} + \delta \left( H^2 \frac{\partial^2 \theta}{\partial t^2} + \frac{R^2}{H^2} \frac{\partial^2 \theta}{\partial y^2} + 2R \frac{\partial^2 \theta}{\partial y \partial t} \right) \\ = \left( \frac{A_4}{A_3} + \frac{4}{3} \frac{Rd}{A_3} \right) \frac{1}{Pr} \frac{\partial^2 \theta}{\partial y^2} \\ + \left( \frac{A_2}{A_3} + K \right) Ec \left( \frac{\partial u}{\partial y} \right)^2 + \left( \frac{A_5}{A_3} \right) Ec M^2 u^2 + \frac{Q}{A_3} \theta. \end{aligned} \quad (11)$$

Where,  $A_1 = (1 - \phi) + \phi \frac{\rho_s}{\rho_f}$ ,  $A_2 = \frac{1}{(1 - \phi)^{2.5}}$ ,  $A_3 = (1 - \phi) + \phi \frac{(\rho C_p)_s}{(\rho C_p)_f}$ ,  $A_4 = \frac{k_s + 2k_f - 2\phi(k_f - k_s)}{k_s + 2k_f + \phi(k_f - k_s)}$ ,  $A_5 = 1 + \frac{3(\frac{\sigma_s}{\sigma_f} - 1)}{(\frac{\sigma_s}{\sigma_f} + 2) - (\frac{\sigma_s}{\sigma_f} - 1)\phi}$ ,  $A_6 = (1 - \phi) + \phi \frac{(\rho\beta)_s}{(\rho\beta)_f}$ ,  $H = \frac{h\sqrt{\omega}}{\nu_f}$  is the frequency parameter,  $R = \frac{v_0 h}{\nu}$  is cross flow Reynolds number,  $Ec = \frac{v_0^2}{(C_p)_f(T_1 - T_0)}$  is the Eckert number,  $\delta = \omega\lambda_2$

is thermal relaxation time parameter,  $M = B_0 h \sqrt{\frac{\sigma_f}{\mu_f}}$  is Hartmann number,  $n = \frac{K_1 h^2}{\gamma}$  is gyration parameter,  $K = \frac{K_1}{\mu_f}$  is coupling parameter,  $P_r = \frac{(\rho C_p)_f \nu_f}{k_f}$  is the Prandtl number,  $Rd = \frac{4\sigma T^3}{k_f k}$  is the radiation

parameter,  $Q = \frac{Q_0 h^2}{(\rho C_p)_f \nu_f}$  is the heat source/sink parameter,  $P_j = \frac{j\mu_f}{\gamma}$  is micro-inertia parameter.

The appropriate B.Cs are,

$$u(0) = 0, \quad N(0) = 0, \quad \theta(0) = 0, \quad (12)$$

$$u(1) = 0, \quad N(1) = 0, \quad \theta(1) = 1. \quad (13)$$

### 3. Solution of the problem

Since the flow is driven by the pressure gradient, the dimensionless pressure gradient is taken as

$$-\frac{\partial P}{\partial x} = \lambda_0 + \varepsilon \lambda_1 e^{it}. \quad (14)$$

Now that the pressure gradient induces the pulsatile flow described in Eq. (14), the velocity  $u$ , microrotation  $N$ , and temperature  $\theta$  are taken as,

$$u = u_0(y) + \varepsilon u_1(y)e^{it}, \quad (15)$$

$$N = N_0(y) + \varepsilon N_1(y)e^{it}, \quad (16)$$

$$\theta = \theta_0(y) + \varepsilon \theta_1(y)e^{it}. \quad (17)$$

By taking the Eqs. (14)–(17) in Eqs. (9)–(11) and equating the corresponding coefficients of  $\varepsilon$  ( $\varepsilon < 1$ ) for different powers of  $\varepsilon$ , we can attain the set of ordinary differential equations

$$\begin{aligned} \left(\frac{A_2 + K}{A_1}\right) u_0'' - Ru_0' - \left(\frac{A_5}{A_1}\right) M^2 u_0 + \frac{A_6}{A_1} \left(\frac{Gr}{Re}\right) (\theta_0) + \frac{K}{A_1} N_0' \\ + \frac{\lambda_0}{A_1} = 0, \end{aligned} \quad (18)$$

$$\left(\frac{A_2 + K}{A_1}\right) u_1'' - Ru_1' - (H^2 i) u_1 - \left(\frac{A_5}{A_1}\right) M^2 u_1 + \frac{A_6}{A_1} \left(\frac{Gr}{Re}\right) (\theta_1)$$

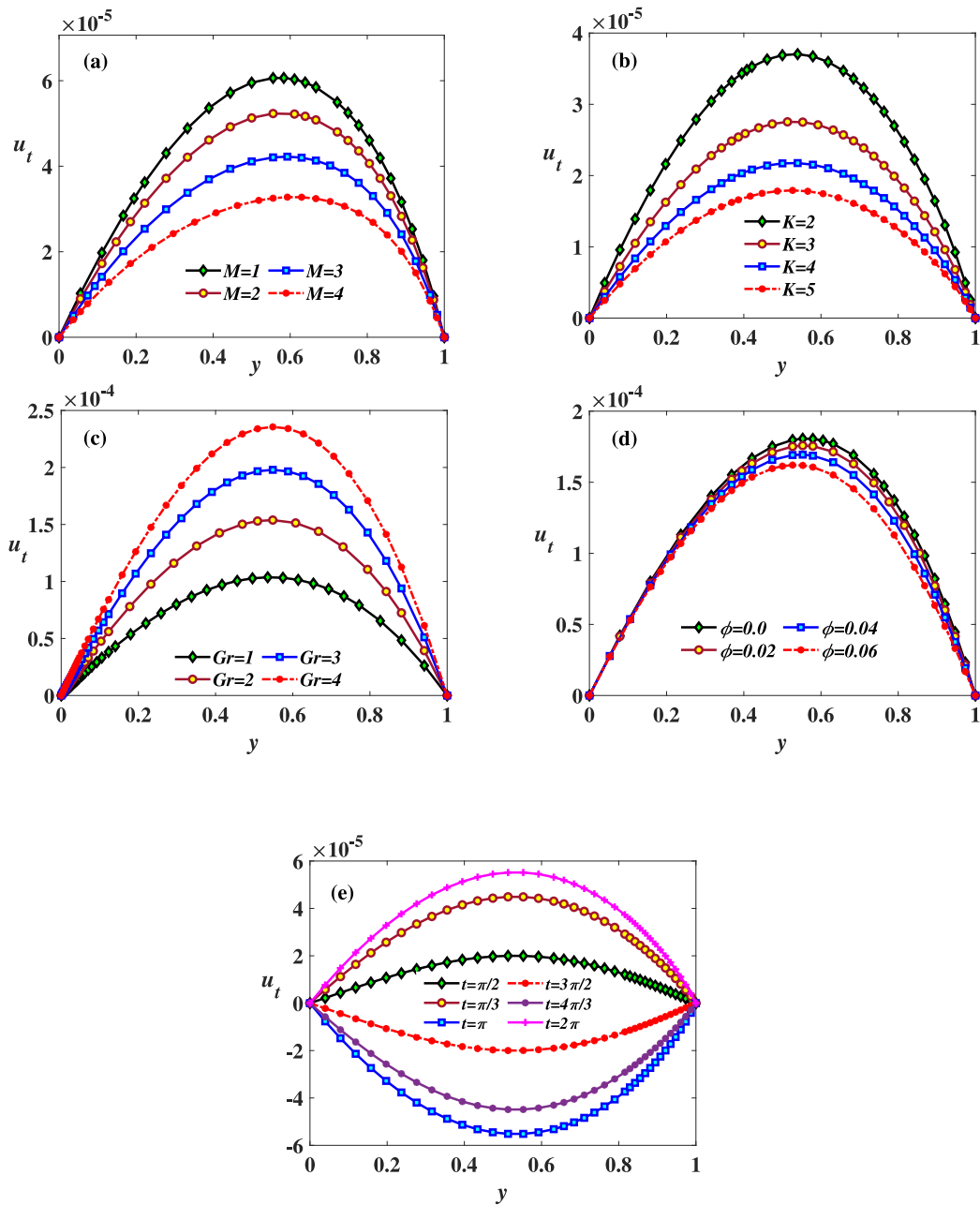


Fig. 3. (a) Impression of  $M$  on  $u_t$ , (b) Impression of  $K$  on  $u_t$ , (c) Impression of  $Gr$  on  $u_t$ , (d) Impression of  $\phi$  on  $u_t$ , (e) Impression of  $t$  on  $u_t$ .

$$+\frac{K}{A_1} N_1' + \frac{\lambda_1}{A_1} = 0, \quad (19)$$

$$\left(\frac{1}{A_1}\right) N_0'' - (P_j R) N_0' - \frac{n}{A_1} u_0' - \left(\frac{2n}{A_1}\right) N_0 = 0, \quad (20)$$

$$\left(\frac{1}{A_1}\right) N_1'' - (P_j R) N_1' - \frac{2n}{A_1} (N_1) - (P_j H^2 i) N_1 - \frac{n}{A_1} u_1' = 0, \quad (21)$$

$$\frac{1}{Pr} \left(\frac{A_4}{A_3} + \frac{4}{3} \frac{Rd}{A_3} - \delta \left(\frac{R^2}{H^2}\right)\right) \theta_0'' + \frac{Q}{A_3} \theta_0 - R\theta_0' + \left(\frac{A_5}{A_3}\right) Ec M^2 u_0^2 + \left(\frac{A_2}{A_3} + K\right) Ec (u_0')^2 = 0, \quad (22)$$

$$\frac{1}{Pr} \left(\frac{A_4}{A_3} + \frac{4}{3} \frac{Rd}{A_3} - \delta \left(\frac{R^2}{H^2}\right)\right) \theta_1'' - R\theta_1' - \delta 2 Ri (\theta_1') + \left(\frac{Q}{A_3}\right) \theta_1 - \delta i H^2 (\theta_1) - \delta i^2 H^2 (\theta_1) + 2 \left(\frac{A_2}{A_3} + K\right) Ec (u_0' u_1') + 2 \left(\frac{A_5}{A_3}\right) M^2 u_0 u_1 = 0. \quad (23)$$

The appropriate B.Cs are

$$u_0 = 0, N_0 = 0, \theta_0 = 0; \quad u_1 = 0, N_1 = 0, \theta_1 = 0 \quad \text{at } y = 0, \quad (24)$$

$$u_0 = 0, N_0 = 0, \theta_0 = 1; \quad u_1 = 0, N_1 = 0, \theta_1 = 0 \quad \text{at } y = 1. \quad (25)$$

The significant physical amount of heat transfer rate at the walls is given in terms of the non-dimensional Nusselt number as,

$$Nu = \left(A_4 + \frac{4}{3} Rd\right) \left(\frac{\partial \theta}{\partial y}\right)_{y=0,1} \quad (26)$$

Now, using MATLAB software and the Runge–Kutta fourth order approach, the system of Eqs. (18)–(23) in associated with B.Cs (24) and (25) is numerically determined. The step size has been set to 0.001 ( $\Delta y = 0.001$ ). For the converging criteria, the accuracy is set at  $1 \times 10^{-10}$ .

To ensure the precision of the current outcomes a comparison has been done between the current outcomes and the outcomes attained by NDSolve using MATHEMATICA which are prearranged in Table 2.

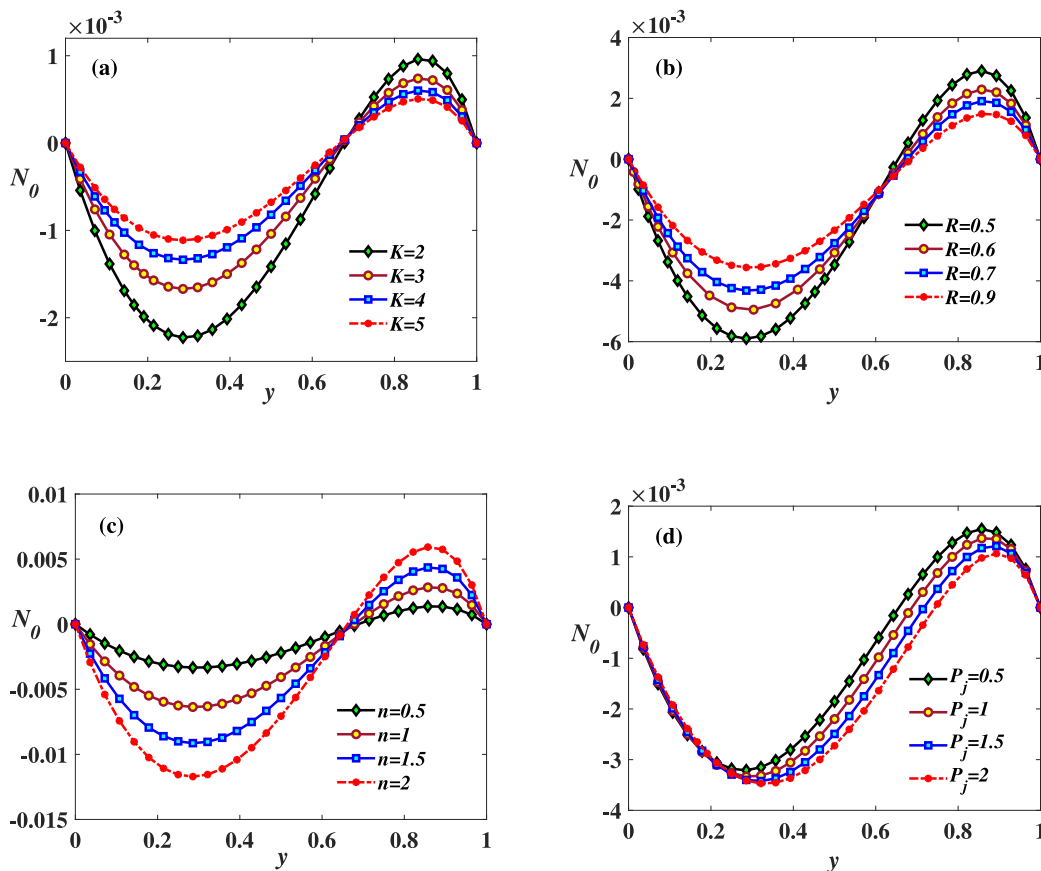


Fig. 4. (a) Impression of  $K$  on  $N_0$  (b) Impression of  $R$  on  $N_0$  (c) Impression of  $n$  on  $N_0$  (d) Impression of  $P_j$  on  $N_0$ .

Table 2

Comparison of present findings and the outcomes of NDSolve for  $(\theta'_0)$  at the wall ( $y = 0$ ) when  $t = \frac{\pi}{4}$ ,  $Q = 0.5$ ,  $K = 0.5$ ,  $Pr = 21$ ,  $H = 3$ ,  $Rd = 1$ ,  $\epsilon = 0.1$ ,  $R = 1$ ,  $\delta = 0.5$ ,  $M = 0.5$ ,  $\varphi = 0.05$ ,  $Ec = 0.5$ ,  $\lambda_0 = 1$ , and  $\lambda_1 = 1$ .

Parameter	Values	Present results	NDSolve
$Ec$	0.1	0.01284863	0.01284878
	0.3	0.03646625	0.03646624
	0.5	0.06241876	0.06241877
	1	0.06241876	0.06241877
$Rd$	2	0.10616575	0.10616575
	3	0.18652950	0.18653816

It is witnessed that there is a worthy settlement between the current outcomes and the outcomes attained by NDSolve. It can be seen that there is a worthy limitation between the current outcomes and the NDSolve outcomes.

### 3.1. Analysis of entropy generation

$$Ns = \frac{K_{nf}}{T_0^2} \left[ 1 + \frac{16\sigma T_0^3}{3kk_f} \right] \left( \frac{\partial \tilde{T}}{\partial \tilde{y}} \right)^2 + \left( \frac{\mu_{nf} + K_1}{T_0} \right) \left( \frac{\partial \tilde{u}}{\partial \tilde{y}} \right)^2 + \left( \frac{\sigma_{nf} B_0^2}{T_0} \right) \tilde{u}^2. \quad (27)$$

The rate of dimensionless entropy generation is in the form

$$NG = A_4 \left( 1 + \frac{4Rd}{3} \right) \left( \frac{\partial \theta}{\partial y} \right)^2 + \frac{A_5 M^2 Ec Pr}{\eta} u^2 + \left( \frac{A_2 Ec Pr K}{\eta} \right) \left( \frac{\partial u}{\partial y} \right)^2, \quad (28)$$

where,  $\eta = \frac{T_1 - T_0}{T_1}$  is the temperature difference, On aspect of Eq. (10), the impression for  $NG$  can be defined as.

$$NG(y) = NG_0(y) + \epsilon NG_1(y)e^{it}, \quad (29)$$

Since by taking Eqs. (15), (16), (17), and (29) into Eq. (27), and taking the coefficients power of  $\epsilon$  into consideration, we get

$$NG_0 = A_4 \left( 1 + \frac{4Rd}{3} \right) (\theta'_0)^2 + \frac{A_5 M^2 Ec Pr}{\eta} u_0^2 + \frac{A_2 K Ec Pr}{\eta} (u'_0)^2, \quad (30)$$

$$NG_1 = 2A_4 \left( 1 + \frac{4Rd}{3} \right) \theta'_0 \theta'_1 + \frac{2A_5 M^2 Ec Pr}{\eta} u_0 u_1 + \frac{2A_2 Ec Pr K}{\eta} u'_0 u'_1, \quad (31)$$

$$Be = \frac{A_4 \left( 1 + \frac{4Rd}{3} \right) \left( \frac{\partial \theta}{\partial y} \right)^2}{NG} \quad (32)$$

### 4. Results and discussion

In this segment, the impacts of Hartmann number ( $M$ ), coupling parameter ( $K$ ), Grashof number ( $Gr$ ), gyration parameter ( $n$ ), cross-flow Reynolds number ( $R$ ), micro-inertia parameter ( $P_j$ ), viscous dissipation ( $Ec$ ), thermal radiation ( $Rd$ ), heat source/sink ( $Q$ ), frequency parameter ( $H$ ), Bejan number ( $Be$ ), entropy generation ( $NG$ ) on steady and unsteady distributions of velocity, microrotation, temperature distribution, heat transfer rate, entropy generation and Bejan number for blood-based micropolar nanofluid with  $Fe_3O_4$  nanoparticles are presented graphically and discussed in detail Figs. 2–10. For the simulation of numerical outcomes, we have taken the standard values adjusted at  $H = 3, R = 1, M = 0.5, Rd = 1, \delta = 0.5, Pr = 21, Gr = 3, t = \pi/4, Rd = 2, Ec = 0.5, n = 0.5, \lambda_0 = \lambda_1 = 1 = P_j = K = 1, Q = 0.5$

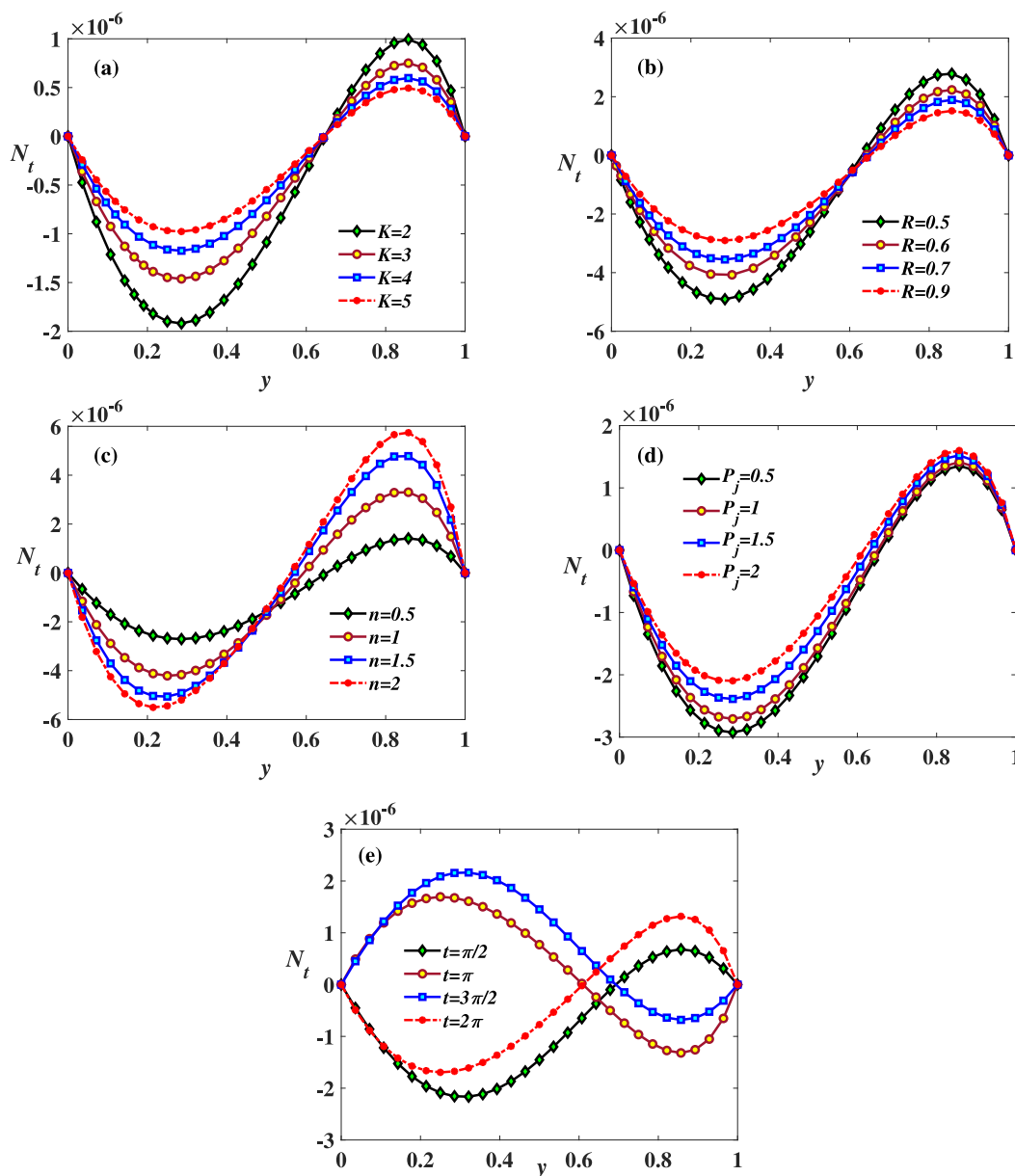


Fig. 5. (a) Impression of  $K$  on  $N_t$  (b) Impression of  $R$  on  $N_t$  (c) Impression of  $n$  on  $N_t$  (d) Impression of  $P_j$  on  $N_t$  (e) Impression of  $t$  on  $N_t$ .

and  $\phi = 0.05$ . Apart from changing the parameters' values as shown in the appropriate figures and tables, these standards are kept constant throughout the study. The influences of the steady velocity distribution in the walls are presented graphically in Fig. 2(a)–(b). Fig. 2(a) demonstrates that the steady velocity ( $u_0$ ) is trending down with an augmentation of the Hartmann number. This could be addressed by the Lorentz force, which is produced by an applied magnetic field and behaves perpendicularly to the direction of the flowing stream. Consequentially, steady velocity is reduced. Fig. 2(b) depict that the variations for steady velocity ( $u_0$ ) is lessening as the coupling parameter value increases. This is because the coupling factor is conflicting the flowing fluid. Thus, the behavior of steady velocity leads to decreasing tendency. Fig. 2(c) exhibit the impression of steady velocity ( $u_0$ ) which is increasing by boosting up the Grashof number. Due to the buoyant force's effectiveness in resisting gravity and it leads to boosts the fluid flow. Fig. 2(d) shows the influence of steady velocity ( $u_0$ ) which is reduced with an increment of the nanoparticle volume fraction. This is due to the density extension of the base fluid with nanoparticles which dignified to decelerate the fluid flow.

The variations of unsteady velocity ( $u_t$ ) for numerous parameters such as Hartmann number ( $M$ ), coupling parameter ( $K$ ), Grashof number ( $Gr$ ), volume fraction of nanoparticles ( $\phi$ ), and time ( $t$ ) are portrayed graphically in Fig. 3(a)–3(e). Fig. 3(a) reveal the unsteady velocity ( $u_t$ ) of micropolar nanofluid is diminished with an amplifying Hartmann number. Since the retarding forces produced by a magnetic field, which responds as a conductive drag force and causes the unsteady velocity ( $u_t$ ) of nanofluid to slow down. By increasing of coupling parameter then the unsteady velocity is in the stage of reducing tendency which is given in Fig. 3(b). The opposite behavior have obtained due to enhancing the values of Grashof number which is presented in Fig. 3(c). In Fig. 3(d) demonstrates the effect of unsteady velocity ( $u_t$ ), which increased as the nanoparticle volume fraction increased. This is due to the addition of nanoparticles to the base fluid, which increases density and elevates the fluid flow. Fig. 3(e) reveal that the unsteady velocity ( $u_t$ ) oscillates with varying the values of time ( $t$ ).

The differences of steady microrotation ( $N_0$ ) is depicted by utilizing the different physical parameters such as cross-flow Reynolds number ( $R$ ), coupling parameter ( $K$ ), gyration parameter ( $n$ ) and micro-inertia

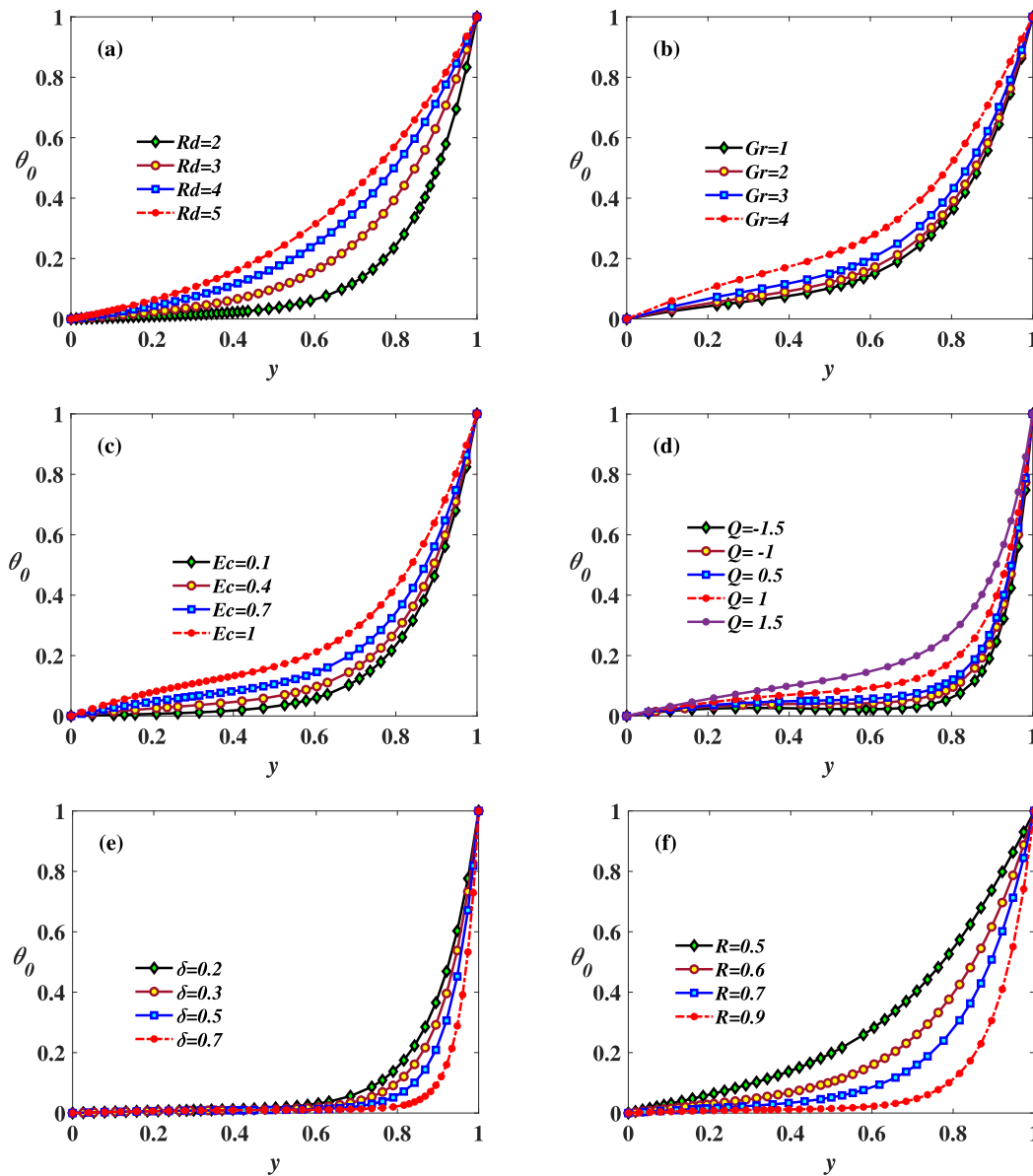


Fig. 6. (a) Impression of  $Rd$  on  $\theta_0$  (b) Impression of  $Gr$  on  $\theta_0$  (c) Impression of  $Ec$  on  $\theta_0$  (d) Impression of  $Q$  on  $\theta_0$  (e) Impression of  $\delta$  on  $\theta_0$  (f) Impression of  $R$  on  $\theta_0$ .

( $P_j$ ) are portrayed in Fig. 4(a)–4(d). Fig. 4(a) exhibits a continuous microrotation that ascends near to the left wall and descends over to the left wall as the coupling parameter is increased. This is because such an influence opposes the fluid flow and causes variations in the flow. Fig. 4(b) depicts that the steady microrotation is rising at the left wall and dwindling in the right wall with the increment of the cross-flow Reynolds number. The opposite nature is happened by boosting the gyration parameter. Since this micro-gyration vector is related to shear stress once fluid is substantiated, it causes to oscillating in the fluid flow. which is plotted in Fig. 4(c). Fig. 4(d) exhibits the steady microrotation is gradually decreasing with the enhancement of the micro-inertia parameter.

The influences of unsteady microrotation ( $Nt$ ) by utilizing the different physical parameters such as cross-flow Reynolds number ( $R$ ), coupling parameter ( $K$ ), gyration parameter micro-inertia ( $P_j$ ) and time ( $t$ ) are portrayed on Fig. 5(a)–5(e). Figs. 5(a) and 5(b) shows the unsteady microrotation is reduced at the lower wall, similarly, it is rising gradually at the right wall with the enhancement of coupling parameter and cross-flow Reynolds number. Fig. 5(c) presents the unsteady microrotation is wavering and decreasing at the left wall also

escalating at the right wall by growing the gyration parameter value. The enhancement of micro-inertia then the unsteady microrotation of micropolar nanofluid is oscillating consequently which is given in Fig. 5(d). In Fig. 5(e) exhibits that the unsteady temperature is oscillating periodically by varying the values of time ( $t$ ).

The influences of steady temperature ( $\theta_0$ ) exhibited by varying the values of emerging physical parameters of thermal radiation ( $Rd$ ), Hartmann number ( $M$ ), viscous dissipation ( $Ec$ ), heat source/sink ( $Q$ ), thermal relaxation parameter ( $\delta$ ), and frequency distribution ( $H$ ) are displayed in Fig. 6(a)–6(f). In Fig. 6(a) depicts that the steady temperature is amplified by rising values of thermal radiation due to such parameter playing an effective role in conducting the heat on the wall and its states to enhance the temperature effect. Fig. 6(b) shows that magnifying the Hartmann number decreases the steady temperature of micropolar nanofluid. The reason is retarding force is generated to create an applied magnetic field that play a role as a frictional drag force and it causes to reduce the steady temperature. Fig. 6(c) reveals that the stable temperature is falling with higher values of the viscous dissipation parameter. This is because the increased Eckert number dissipates greater energy in the system. In Fig. 6(d) reveal that the

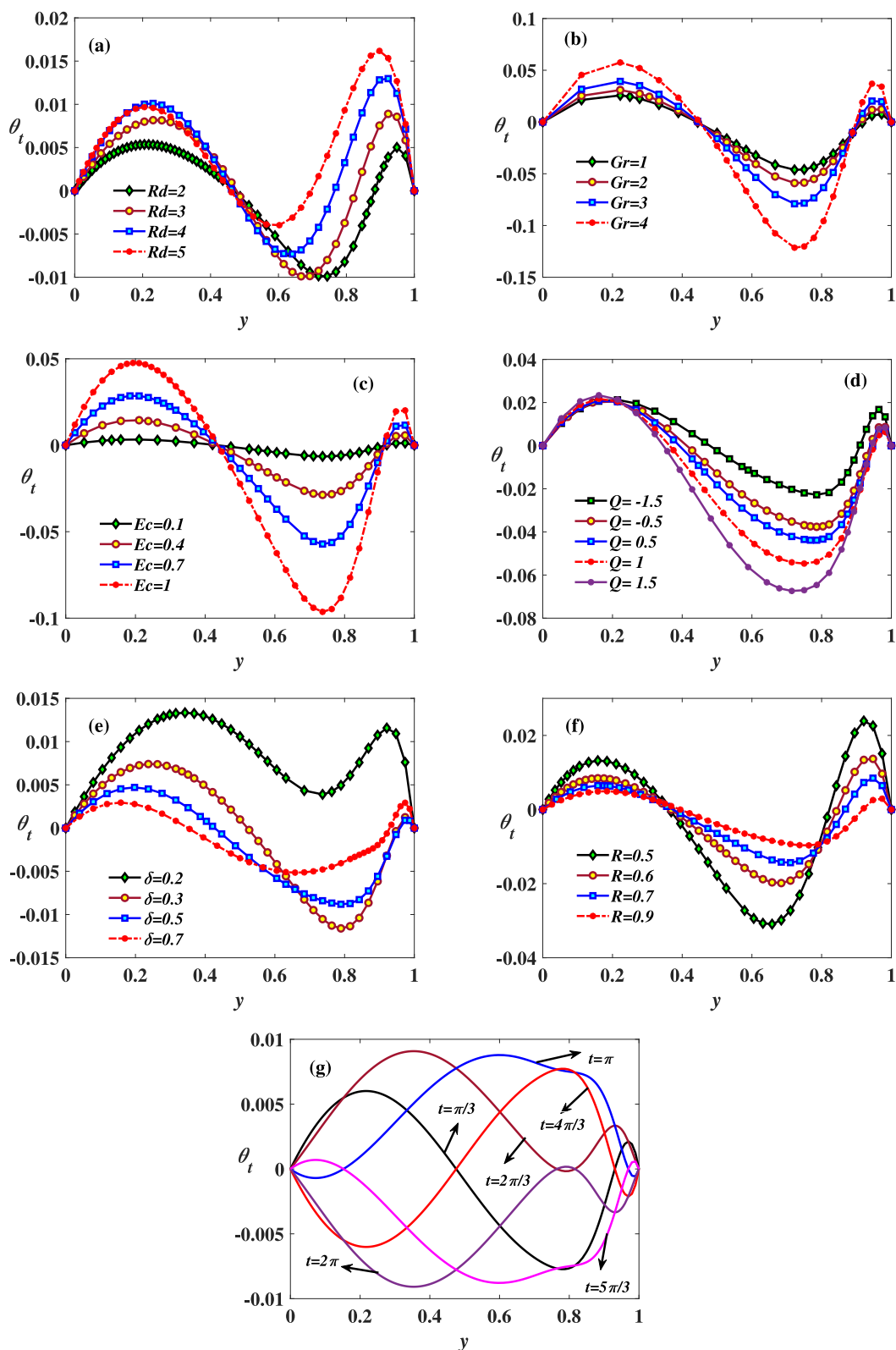


Fig. 7. (a) Impression of  $Rd$  on  $\theta_t$ , (b) Impression of  $Gr$  on  $\theta_t$ , (c) Impression of  $Ec$  on  $\theta_t$ , (d) Impression of  $Q$  on  $\theta_t$ , (e) Impression of  $\delta$  on  $\theta_t$ , (f) Impression of  $R$  on  $\theta_t$ , (g) Impression of  $t$  on  $\theta_t$ .

unsteady temperature is increasing in according to increment of heat source ( $Q > 0$ ), similarly, the temperature is increasing by boosting up the heat sink values ( $Q < 0$ ). The temperature of micropolar nanofluid is

decreasing due to an increase in the thermal relaxation effect. Because computable particles have a larger likelihood of giving heat to their nearby particles as the relaxation time parameter of heat flux increases,

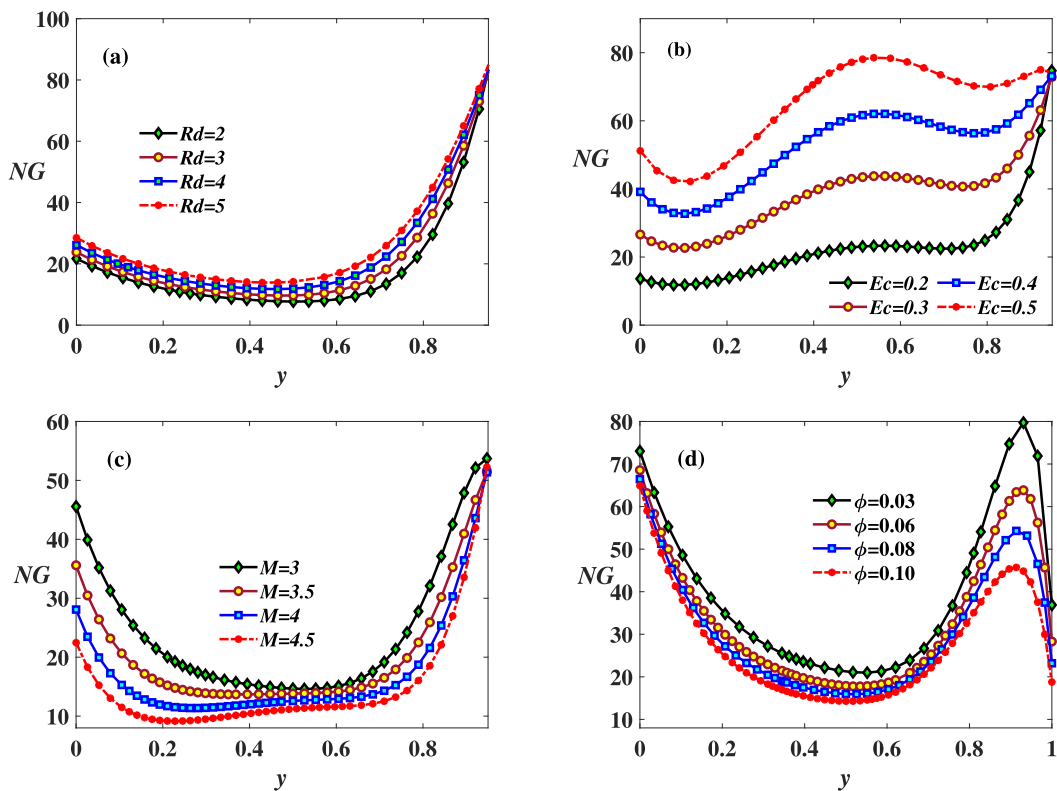


Fig. 8. (a) Impression of  $Rd$  on  $NG$  (b) Impression of  $Ec$  on  $NG$  (c) Impression of  $M$  on  $NG$  (d) Impression of  $\phi$  on  $NG$ .

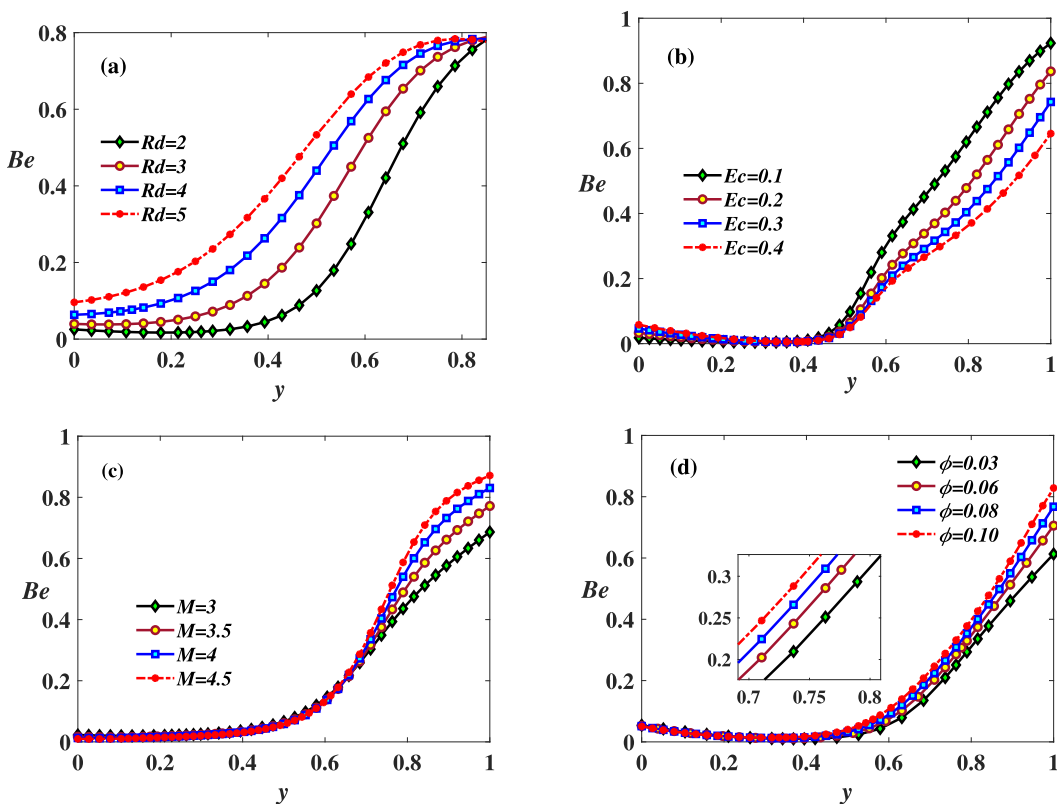


Fig. 9. (a) Impression of  $Rd$  on  $Be$  (b) Impression of  $Ec$  on  $Be$  (c) Impression of  $M$  on  $Be$  and (d) Impression of  $\phi$  on  $Be$ .

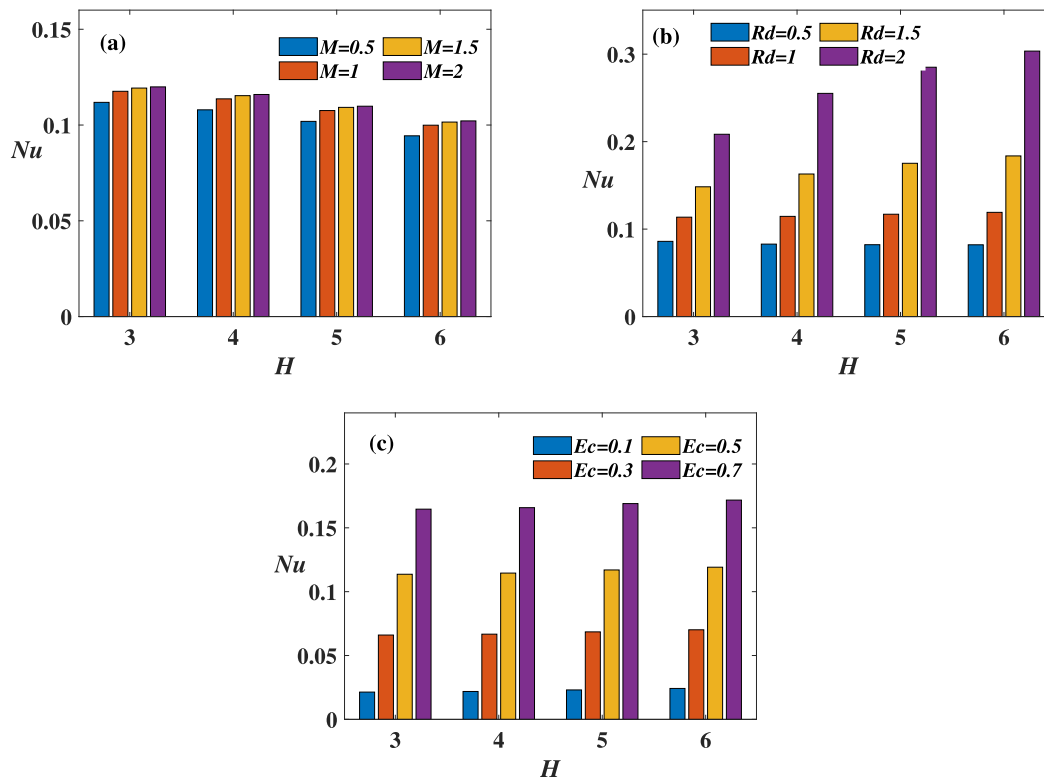


Fig. 10. Distributions of heat transfer rate (Nusselt number) against  $H$ : (a) Impression of  $M$  (b) Impression of  $Rd$  and (c) Impression of  $Ec$ .

energy is lowered, as seen in Fig. 6(e). The same behavior is obtained in Fig. 6(f) with an enhancement of cross-flow Reynolds number.

The influences of unsteady temperature ( $\theta_t$ ) are demonstrated by applying various physical parameters of thermal radiation ( $Rd$ ), Hartmann number ( $M$ ), viscous dissipation ( $Ec$ ), heat source/sink ( $Q$ ), thermal relaxation parameter ( $\delta$ ), frequency distribution ( $H$ ), and time ( $t$ ) are portrayed in Fig. 7(a)–7(g). In Fig. 7(a) shows that the unsteady temperature is oscillating and increasing near to the right wall with an increment of the thermal radiation parameter. By enhancing the Hartmann number then, the unsteady temperature is ascending at the left and right wall at the same time it is descending in the middle of the channel which is presented in Fig. 7(b). The opposite nature has been obtained by rising the values of viscous dissipation as plotted in Fig. 7(c). In Fig. 7(d) shows that the unsteady temperature is dwindling when accelerating heat source ( $Q > 0$ ) while it is amplifying with the decrement of a heat sink ( $Q < 0$ ) parameter. Fig. 7(e) depicts that the unsteady temperature is diminishing and oscillating periodically by the enhancement of the thermal relaxation effect. Fig. 7(f) portrays that the unsteady temperature of micropolar nanofluid is wavering and increasing in the center of the channel by accelerating the cross-flow Reynolds number. By varying time ( $t$ ) then the unsteady temperature of micropolar nanofluid is oscillating periodically which is presented in Fig. 7(g) accordingly.

From Fig. 8(a)–8(d) presents the impressions total entropy generation for various parameters such as thermal radiation ( $Rd$ ), viscous dissipation ( $Ec$ ), Hartmann number ( $M$ ), and nanoparticle volume fraction ( $\phi$ ). Fig. 8(a) shows that the variations of entropy is upsurged by giving higher values of thermal radiation, due to the thermal radiation's relative commitment with the conductive heat energy. Fig. 8(b) depicts that entropy is enhanced by increasing the values of viscous dissipation. The same behavior is obtained with the rise of viscous dissipation. Because the entropy generation is enhanced due to the frictional resistance supposed to act on high fluid flow, the collision of liquid flowing serves to enhance entropy. The similar nature is obtained with the growth of Hartmann number, due to magnetic field produces drag

forces, and it causes to changes in entropy generation which is given in Fig. 8(c). Fig. 8(d) exhibits the entropy is diminished by accelerating nanoparticle volume fraction.

The impacts of temperature related Bejan number ( $Be$ ) is incorporated in Fig. 9(a)–9(d) in addition of viscous dissipation, thermal radiation, Hartmann number, and nanoparticle volume fraction. Fig. 9(a) designate the effects of Bejan is accelerates for giving higher values of thermal radiation. Fig. 9(b) shows that the Bejan number is diminishes over to rise of viscous dissipation effect and it is dominating the impacts of fluid non-reversibility process in the walls. Fig. 9(c) explains the effects of the Hartmann number on the Bejan number, it discovered that the increasing nature caused by the Lorentz force acting on the flow results in an increment in the Bejan number. The same nature obtained with giving higher values of nanoparticle volume fraction which is shown in Fig. 9(d).

The influences of heat transfer rate ( $Nu$ ) of micropolar nanofluid at the left wall ( $y = 0$ ) against  $H$  for different physical parameters such as  $M$ ,  $Rd$  and  $Ec$  are given in Fig. 10(a)–10(c). Evidently, one can notice that the heat transfer rate is increasing with the enhancement of Hartmann number against frequency parameter which is given in Fig. 10(a). In Fig. 10(b) shows that total heat transfer rate is upsurged by amplifying the thermal radiation. Fig. 10(c) depicts that the heat transfer rate is accelerates by increasing the values of viscous dissipation against frequency parameter.

The dispersion of heat transfer rate (Nusselt number) for steady and unsteady impacts for the left wall ( $y=0$ ) with the different parameters such as  $Rd$ ,  $K$ ,  $Ec$ , and  $M$  have been presented in Table 3. In given table, the influences of steady ( $Nu_0$ ) and unsteady Nusselt number ( $Nu_t$ ) are accelerated by intensifying the Hartmann number, and coupling parameter in the micropolar nanofluid while they are diminished with an enhancement of  $Rd$  and  $Ec$ .

## 5. Conclusion

The current work investigates that the entropy generation of hydromagnetic pulsating flow of a micropolar nanofluid in between two

**Table 3**

Distributions for steady and unsteady heat transfer rates for  $M, Ec, K, Rd, m$  and  $\delta$  when  $\epsilon = 0.1, t = \frac{\pi}{4}, Ec = 0.5, Pr = 21, K = 1, H = 3, \delta = 0.5, R = 1, Q = 0.5, M = 0.5, n = 0.5, \lambda_0 = 1$ , and  $\lambda_1 = 1$  at the wall ( $y = 0$ ).

Parameter	Values	$(Nu'_0)_{y=0}$	$(Nu''_0)_{y=0}$
M	0.5	0.112404	0.001238
	1	0.104658	0.001185
	1.5	0.093560	0.001104
Ec	0.1	0.021125	0.000234
	0.3	0.065314	0.000721
	0.5	0.112404	0.001238
K	1	0.112404	0.001238
	2	0.079633	0.000976
	3	0.061570	0.000790
Rd	2	0.206432	0.001999
	3	0.516833	0.003409
	4	1.151402	0.005449

vertical porous walls with the occurrence of Cattaneo–Christov heat flux model, viscous dissipation, Ohmic heating, and thermal radiation. Here, blood is considered as base fluid and  $Fe_3O_4$  as nanoparticle. The addressed model is essential in the investigation of nano-drug delivery, pharmaceuticals, polymer engineering, and biological fluid modeling. The obtained results are accomplished by using a shooting approach with the aid of fourth-order Runge–Kutta scheme. The variations of velocity, microrotation, temperature profiles, heat transfer rate, entropy generation and Bejan number of micropolar nanofluid which are explained by revealing figures. The most important outcomes are given below.

- The steady velocity is diminishing with the enhancement of Hartmann number, and nanoparticle volume fraction while it is amplifying for the higher values of Grashof number.
- The impacts of unsteady microrotation is rising over to the left wall and decreasing over to the right wall by increasing coupling parameter, cross-flow Reynolds number and micro-inertia parameter.
- By the enhancement of radiation parameter, and viscous dissipation then steady temperature is increased.
- The nanoparticle volume fraction of micro-rotation is reduced with the increment of angular momentum.
- A total entropy is mounting up by accelerating the values of viscous dissipation and thermal radiation.
- The impacts steady Nusselt number which is magnifying with an intensification of Hartmann number, coupling parameter, and thermal relaxation time parameter.

**Declaration of competing interest**

The authors declare that they have no known competing financial interests or personal relationships that could have appeared to influence the work reported in this paper.

**Data availability**

No data was used for the research described in the article.

**References**

[1] A.C. Eringen, Simple microfluids, *Internat. J. Engrg. Sci.* 2 (1964) 205–217, [http://dx.doi.org/10.1016/0020-7225\(64\)90005-9](http://dx.doi.org/10.1016/0020-7225(64)90005-9).  
 [2] A.C. Eringen, Theory of micropolar fluids, *Internat. J. Engrg. Sci.* 16 (1966) 1–18, <http://dx.doi.org/10.1512/iumj.1967.16.16001>.  
 [3] A.C. Eringen, Theory of thermo-microstretch fluids and bubbly liquids, *Internat. J. Engrg. Sci.* 28 (1990) 133–143, [http://dx.doi.org/10.1016/0020-7225\(90\)90063-O](http://dx.doi.org/10.1016/0020-7225(90)90063-O).

[4] Z. Shah, E.O. Alzahrani, A. Dawar, A. Ullah, I. Khan, Influence of cattaneo-christov model on Darcy-forchheimer flow of micropolar ferrofluid over a stretching/shrinking sheet, *Int. Commun. Heat Mass Transf.* 110 (2020) 104385, <http://dx.doi.org/10.1016/j.icheatmasstransfer.2019.104385>.  
 [5] S. Nadeem, M.N. Khan, N. Muhammad, S. Ahmad, Mathematical analysis of bio-convective micropolar nanofluid, *J. Comput. Des. Eng.* 6 (2019) 233–242, <http://dx.doi.org/10.1016/j.jcde.2019.04.001>.  
 [6] R. Ellahi, The effects of MHD and temperature dependent viscosity on the flow of non-Newtonian nanofluid in a pipe: analytical solutions, *Appl. Math. Model.* 37 (3) (2013) 1451–1467, <http://dx.doi.org/10.1016/j.apm.2012.04.004>.  
 [7] X. Si, L. Zheng, P. Lin, X. Zhang, Y. Zhang, Flow and heat transfer of a micropolar fluid in a porous channel with expanding or contracting walls, *Int. J. Heat Mass Transfer* 67 (2013) 885–895, <http://dx.doi.org/10.1016/j.jheatmasstransfer.2013.08.012>.  
 [8] D. Pal, G. Mandal, Thermal radiation and MHD effects on boundary layer flow of micropolar nanofluid past a stretching sheet with non-uniform heat source/sink, *Int. J. Mech. Sci.* 2 (2017) 308–318, <http://dx.doi.org/10.1016/j.ijmecsci.2016.12.023>.  
 [9] A. Eringen, Simple microfluids, *Internat. J. Engrg. Sci.* 2 (1964) 205–217, [http://dx.doi.org/10.1016/0020-7225\(64\)90005-9](http://dx.doi.org/10.1016/0020-7225(64)90005-9).  
 [10] S. Jaiswal, P.K. Yadav, A micropolar-Newtonian blood flow model through a porous layered artery in the presence of a magnetic field, *Phys. Fluids* 31 (2019) <http://dx.doi.org/10.1063/1.5100802>.  
 [11] A. Zeeshan, N. Shehzad, M. Atif, R. Ellahi, S.M. Sait, Electromagnetic flow of SWCNT/MWCNT suspensions in two immiscible water-and engine-oil-based newtonian fluids through porous media, *Symmetry* 14 (2) (2022) 406, <http://dx.doi.org/10.3390/sym14020406>.  
 [12] K.E. Aslani, I.E. Sarris, Effect of micromagnetorotation on magnetohydrodynamic Poiseuille micropolar flow: Analytical solutions and stability analysis, *J. Fluid Mech.* 920 (2021) 1–26, <http://dx.doi.org/10.1017/jfm.2021.437>.  
 [13] S.U.S. Choi, J. Eastman, Enhancing thermal conductivity of fluids with nanoparticles, *Am. Soc. Mech. Eng. Fluids Eng. Div. FED* 2 (1995) 99–105, [http://dx.doi.org/10.1016/0020-7225\(64\)90005-9](http://dx.doi.org/10.1016/0020-7225(64)90005-9).  
 [14] M.S. Abdel-wahed, Magnetohydrodynamic Ferro-Nano fluid flow in a semi-porous curved tube under the effect of hall current and nonlinear thermal radiative, *J. Magn. Magn. Mater.* 474 (2019) 347–354, <http://dx.doi.org/10.1016/j.jmmm.2018.11.050>.  
 [15] S.S. Ghadikolaei, K. Hosseinzadeh, D.D. Ganji, M. Hatami,  $Fe_3O_4-CH_2OH_2$  nanofluid analysis in a porous medium under MHD radiative boundary layer and dusty fluid, *J. Mol. Liq.* 258 (2018) 172–185, <http://dx.doi.org/10.1016/j.molliq.2018.02.106>.  
 [16] M. Sheikholeslami, D.D. Ganji, M.Y. Javed, R. Ellahi, Effect of thermal radiation on magnetohydrodynamics nanofluid flow and heat transfer by means of two phase model, *J. Magn. Magn. Mater.* 374 (2015) 36–43, <http://dx.doi.org/10.1016/j.jmmm.2014.08.021>.  
 [17] S.A. Shehzad, M.G. Reddy, P. Vijayakumari, I. Tlili, Behavior of ferromagnetic  $Fe_3SO_4$  and titanium alloy  $Ti_6Al_4V$  nanoparticles in micropolar fluid flow, *Int. Commun. Heat Mass Transf.* 117 (2020) <http://dx.doi.org/10.1016/j.icheatmasstransfer.2020.104769>.  
 [18] S. Hajarika, S. Ahmed, A.J. Chamkha, Investigation of nanoparticles Cu, Ag and  $Fe_3O_4$  on thermophoresis and viscous dissipation of MHD nanofluid over a stretching sheet in a porous regime, *Numer. Model. Math. Comput. Simul.* 182 (2021) 819–837, <http://dx.doi.org/10.1016/j.matcom.2020.12.005>.  
 [19] G. Venkatesan, A.S. Reddy, Insight into the dynamics of blood conveying alumina nanoparticles subject to Lorentz force, viscous dissipation, thermal radiation, Joule heating, and heat source, *Eur. Phys. J. Spec. Top.* 123 (2021) <http://dx.doi.org/10.1140/epjs/s11734-021-00052-w>.  
 [20] M. Hassan, A. Zeeshan, A. Majeed, R. Ellahi, Particle shape effects on ferrofluids flow and heat transfer under influence of low oscillating magnetic field, *J. Magn. Magn. Mater.* 443 (2017) 36–44, <http://dx.doi.org/10.1016/j.jmmm.2017.07.024>.  
 [21] T. Hayat, Z. Nisar, A. Alsaedi, Bioconvection and Hall current analysis for peristalsis of nanofluid, *Int. Commun. Heat Mass Transf.* 129 (2021) 105693, <http://dx.doi.org/10.1016/j.icheatmasstransfer.2021.105693>.  
 [22] S. Rajamani, A.S. Reddy, Pulsating flow of electrically conducting couple stress nanofluid in a channel with Ohmic dissipation and thermal radiation – Dynamics of blood, *Proc. Inst. Mech. Eng. E* 235 (2021) 1895–1909, <http://dx.doi.org/10.1177/09544089211025177>.  
 [23] N. Shehzad, A. Zeeshan, M. Shakeel, R. Ellahi, S.M. Sait, Effects of magnetohydrodynamics flow on multilayer coatings of Newtonian and non-Newtonian fluids through porous inclined rotating channel, *Coatings* 12 (4) (2022) 430, <http://dx.doi.org/10.3390/coatings12040430>.  
 [24] B. Sharma, R. Gandhi, M. Bhatti, Entropy analysis of thermally radiating MHD slip flow of hybrid nanoparticles (Au- $Al_2O_3$ /Blood) through a tapered multstenosed artery, *Chem. Phys. Lett.* 2 (1964) 205–217, <http://dx.doi.org/10.1016/j.cplett.2022.139348>.  
 [25] R. Ellahi, F. Hussain, Simultaneous effects of MHD and partial slip on peristaltic flow of Jeffery fluid in a rectangular duct, *J. Magn. Magn. Mater.* 393 (2015) 284–292, <http://dx.doi.org/10.1016/j.jmmm.2015.05.071>.

- [26] T. Malathy, S. Srinivas, Pulsating flow of a hydromagnetic fluid between permeable beds, *Int. Commun. Heat Mass Transfer* 35 (5) (2008) 681–688, <http://dx.doi.org/10.1016/j.icheatmasstransfer.2007.12.006>.
- [27] C.Y. Wang, Pulsatile flow in a porous channel, *J. Appl. Mech. Trans. ASME* 38 (1971) 553–555, <http://dx.doi.org/10.1115/1.3408822>.
- [28] G. Radhakrishnamacharya, M.K. Maiti, Heat transfer to pulsatile flow in a channel, *Int. J. Heat Mass Transfer* 20 (1977) 171–173.
- [29] A.R. Bestman, Pulsatile flow in heated porous channel, *Int. J. Heat Mass Transfer* 25 (1982) 675–682, [http://dx.doi.org/10.1016/0017-9310\(82\)90172-7](http://dx.doi.org/10.1016/0017-9310(82)90172-7).
- [30] M.M. Bhatti, S.M. Sait, R. Ellahi, Magnetic nanoparticles for drug delivery through tapered stenosed artery with blood based non-Newtonian fluid, *Pharmaceuticals* 15 (11) (2022) 1352, <http://dx.doi.org/10.3390/ph15111352>.
- [31] P. Bitla, T.K.V. Iyengar, Pulsating flow of an incompressible micropolar fluid between permeable beds with an inclined uniform magnetic field, *Internat. J. Engrg. Sci.* 48 (1964) 174–182, <http://dx.doi.org/10.1016/j.euromechflu.2014.06.002>.
- [32] S. Akar, J.A. Esfahani, S.A.M. Shaegh, A numerical investigation of magnetic field effect on blood flow as biomagnetic fluid in a bend vessel, *J. Magn. Magn. Mater.* 482 (2019) 336–349, <http://dx.doi.org/10.1016/j.jmmm.2019.03.043>.
- [33] G.C. Shit, S. Maiti, J.C.M. M Roy, Pulsatile flow and heat transfer of blood in an overlapping vibrating atherosclerotic artery: A numerical study, *Math. Comput. Simulation* 166 (2019) 432–450, <http://dx.doi.org/10.1016/j.matcom.2019.06.015>.
- [34] C.K. Kumar, S. Srinivas, A.S. Reddy, MHD pulsating flow of casson nanofluid in a vertical porous space with thermal radiation and Joule heating, *J. Mech.* 36 (1964) 535–549, <http://dx.doi.org/10.1017/jmech.2020.5>.
- [35] D. Rajkumar, A.S. Reddy, Pulsating electrically conducting flow of Au/SWCNTs-blood micropolar nanofluid in a porous channel with Ohmic heating, thermal radiation, *Phys. Scr.* 96 (2021) 125233, <http://dx.doi.org/10.1088/1402-4896/ac2e81>.
- [36] M.A.E. Kot, Y.A. Elmaboud, Unsteady pulsatile fractional Maxwell viscoelastic blood flow with cattaneo heat flux through a vertical stenosed artery with body acceleration, *J. Therm. Anal. Calorim.* (2021) <http://dx.doi.org/10.1007/s10973-021-10822-2>.
- [37] K. Govindarajulu, A.S. Reddy, Magnetohydrodynamic pulsatile flow of third grade hybrid nanofluid in a porous channel with ohmic heating and thermal radiation effects, *Phys. Fluids* 34 (2022) <http://dx.doi.org/10.1063/5.0074894>.
- [38] C. Cattaneo, On heat conduction, *Atti Sem. Mat. Fis. Univ. Modena* (1948) 83–101, <http://ci.nii.ac.jp/naid/10030920715/en/>. (Accessed November 8, 2021).
- [39] C.I. Christov, On frame indifferent formulation of the Maxwell-Cattaneo model of finite-speed heat conduction, *Mech. Res. Commun.* 36 (2009) 481–486, <http://dx.doi.org/10.1016/j.mechrescom.2008.11.003>.
- [40] T. Hayat, T. Ayub, T. Muhammad, B. Ahmad, Nonlinear computational treatment for couple stress fluid flow with Cattaneo-Christov double diffusion and homogeneous-heterogeneous reactions, *Int. J. Chem. React. Eng.* 17 (2019) 1–14, <http://dx.doi.org/10.1515/ijcre-2018-0056>.
- [41] A. Majeed, A. Zeeshan, M.M. Bhatti, R. Ellahi, Heat transfer in magnetite (Fe<sub>3</sub>O<sub>4</sub>) nanoparticles suspended in conventional fluids: Refrigerant-134A (CH<sub>2</sub>F<sub>2</sub>), kerosene (C<sub>10</sub>H<sub>22</sub>), and water (H<sub>2</sub>O) under the impact of dipole, *Heat Transfer Res.* 51 (3) (2020) <http://dx.doi.org/10.1615/HeatTransRes.2019029919>.
- [42] A.U. Yahya, N. Salamat, D. Habib, B. Ali, S. Hussain, S. Abdal, Simple microfluidic, *Internat. J. Engrg. Sci.* 2 (1964) 205–217, [http://dx.doi.org/10.1016/0020-7225\(64\)90005-9](http://dx.doi.org/10.1016/0020-7225(64)90005-9).
- [43] A. Mahmood, B. Chen, A. Ghaffari, Hydromagnetic hhiemenz flow of micropolar fluid over a nonlinearly stretching/shrinking sheet: Dual solutions by using Chebyshev Spectral Newton Iterative Scheme, *J. Magn. Magn. Mater.* 416 (2016) 329–334, <http://dx.doi.org/10.1016/j.jmmm.2016.05.001>.
- [44] E.O. Fatunmbi, A. Adeniyani, Nonlinear thermal radiation and entropy generation on steady flow of magneto-micropolar fluid passing a stretchable sheet with variable properties, *Results Eng.* 6 (2020) 100142, <http://dx.doi.org/10.1016/j.rineng.2020.100142>.
- [45] M. Hatami, J. Hatami, D.D. Ganji, Computer simulation of MHD blood conveying gold nanoparticles as a third grade non-Newtonian nanofluid in a hollow porous vessel, *Comput. Methods Programs Biomed.* 113 (2014) 632–641, <http://dx.doi.org/10.1016/j.cmpb.2013.11.001>.
- [46] M. Bhatti, O.A. Bég, R. Ellahi, M. Doranehgard, F. Rabiei, Electromagnetohydrodynamics hybrid nanofluid flow with gold and magnesium oxide nanoparticles through vertical parallel plates, *J. Magn. Magn. Mater.* 564 (2022) 170136, <http://dx.doi.org/10.3390/ph15111352>.
- [47] M.S. Abdel-Wahed, Rotating ferro-nanofluid over stretching plate under the effect of hall current and Joule heating, *J. Magn. Magn. Mater.* 429 (2017) 287–293, <http://dx.doi.org/10.1016/j.jmmm.2017.01.032>.
- [48] K. Al-Khaled, M. Khan, S. Khan, M. Malik, S. Qayyum, Non-uniform heat source/sink applications for the radiative flow of Brinkman micropolar nanofluid with microorganisms, *Comput. Theor. Chem.* 2 (2021) 205–217, <http://dx.doi.org/10.1016/j.comptc.2021.113330>.
- [49] S. Asha, C. Deepa, Entropy generation for peristaltic blood flow of a magneto-micropolar fluid with thermal radiation in a tapered asymmetric channel, *Results Eng.* 3 (2019) 100024, <http://dx.doi.org/10.1016/j.rineng.2019.100024>.
- [50] P.K. Yadav, A. Kumar, An inclined magnetic field effect on entropy production of non-immiscible Newtonian and micropolar fluid in a rectangular conduit, *Int. Commun. Heat Mass Transf.* 124 (2021) 105266, <http://dx.doi.org/10.1016/j.icheatmasstransfer.2021.105266>.
- [51] T.A. Yusuf, R.N. Kumar, B.C. Prasannakumara, S.O. Adesanya, Irreversibility analysis in micropolar fluid film along an incline porous substrate with slip effects, *Int. Commun. Heat Mass Transf.* 126 (2021) 105357, <http://dx.doi.org/10.1016/j.icheatmasstransfer.2021.105357>.
- [52] T. Hayat, S. Qayyum, M.I. Khan, A. Alsaedi, Entropy generation in magnetohydrodynamic radiative flow due to rotating disk in presence of viscous dissipation and Joule heating, *Phys. Fluids* 30 (2018) 205–217, <http://dx.doi.org/10.1063/1.5009611>.
- [53] X. Chen, Y. Jian, Entropy generation minimization analysis of two immiscible fluids, *Int. J. Therm. Sci.* 171 (2022) 107210, <http://dx.doi.org/10.1016/j.jthermalsci.2021.107210>.